nanomaterials

MDPI

Review

Hetero-Element-Doped Molybdenum Oxide Materials for Energy Storage Systems

Bo Hu [1,2], Shuofeng Jian [1], Ge Yin [1], Wenhao Feng [1], Yaowen Cao [1], Jiaxuan Bai [1], Yanan Lai [1], Huiyun Tan [1,*] and Yifan Dong [1,*]

[1] Engineering Research Center of Nano-Geomaterials of Ministry of Education, Faculty of Material Science and Chemistry, China University of Geosciences, Wuhan 430074, China; hubocug@cug.edu.cn (B.H.); jianshuofeng@163.com (S.J.); yinge3111818157@126.com (G.Y.); wenhaofeng5@gmail.com (W.F.); caoyaowen12@163.com (Y.C.); Phoenix9360@yeah.net (J.B.); nannan2002617@163.com (Y.L.)

[2] Faculty of Material Science and Chemistry, China University of Geosciences, Wuhan 430074, China

* Correspondence: thy98_cug@163.com (H.T.); dongyf@cug.edu.cn (Y.D.)

Abstract: In order to meet the growing demand for the electronics market, many new materials have been studied to replace traditional electrode materials for energy storage systems. Molybdenum oxide materials are electrode materials with higher theoretical capacity than graphene, which was originally used as anode electrodes for lithium-ion batteries. In subsequent studies, they have a wider application in the field of energy storage, such as being used as cathodes or anodes for other ion batteries (sodium-ion batteries, potassium-ion batteries, etc.), and electrode materials for supercapacitors. However, molybdenum oxide materials have serious volume expansion concerns and irreversible capacity dropping during the cycles. To solve these problems, doping with different elements has become a suitable option, being an effective method that can change the crystal structure of the materials and improve the performances. Therefore, there are many research studies on metal element doping or non-metal doping molybdenum oxides. This paper summarizes the recent research on the application of hetero-element-doped molybdenum oxides in the field of energy storage, and it also provides some brief analysis and insights.

Keywords: molybdenum oxides; hetero-element doping; energy storage materials

Citation: Hu, B.; Jian, S.; Yin, G.; Feng, W.; Cao, Y.; Bai, J.; Lai, Y.; Tan, H.; Dong, Y. Hetero-Element-Doped Molybdenum Oxide Materials for Energy Storage Systems. *Nanomaterials* **2021**, *11*, 3302. https://doi.org/10.3390/nano11123302

Academic Editor: Marc Cretin

Received: 20 October 2021
Accepted: 22 November 2021
Published: 6 December 2021

1. Introduction

The rapid growth of the population and industrial production have put great pressure on natural resources, and, with the depletion of fossil energy and the rapid development of electronic products, the demands for high energy density and power density energy storage equipment, such as ion batteries and supercapacitors, continues to grow [1–3]. Over the last few decades, lithium-ion batteries (LIBs) have become the favorite in the consumer electronics market due to their good energy density, long cycle life, and environmental friendliness. The abundant mineral materials in nature are used as the matrix for the research of electrode materials for lithium-ion batteries [4]. As we know, transition metal oxides are appropriate for the insertion/extraction of small ions, such as H^+ and Li^+, so they are candidates for a wide range of applications, including energy storage devices [5]. Among the transition metal oxides, molybdenum oxides have diverse crystal structures, oxidation states, and particular physicochemical properties, such as conductivity, mechanical and thermal stability, as well as cyclability [6]. In addition, they are wide band gap n-type semiconductors, which plays a vital role in technological applications [7]. At the same time, graphite materials have been successfully marketed as anodes for LIBs for decades, but the low theoretical specific capacity of 372 mA h g^{-1} has gradually failed to meet the growing demand for high energy density batteries [8,9]. Molybdenum oxide, particularly MoO_2, has received considerable attention due to its metallic conductivity and high theoretical capacity (838 mA h g^{-1}) [10]. Therefore, molybdenum oxides, as

cathode or anode materials, appear to be promising candidates for ion secondary batteries and supercapacitors.

There has been a great deal of research on pure molybdenum oxides using different methods, such as thermal decomposition [11], chemical vapor deposition [12], hydrothermal-solvothermal process [13–15], thermal evaporation, and nanocasting, to synthesize nanostructure molybdenum oxides to increase electrochemical performance. However, the interlamellar spacing of pure molybdenum oxides is limited, it is difficult to enhance their specific capacities, and they cannot hold big ions, such as Na^+, K^+, Zn^{2+}, and Mg^{2+}. Therefore, it is necessary to approach them from another perspective to improve the electrochemical performance of molybdenum oxide-based materials. Doping with different elements is an effective strategy, which can increase the distance between the layers in the crystal structure, change the layered crystal structure to a tunnel-type structure, or enhance conductivity.

Hetero-element doping molybdenum oxides can be divided into several varieties, namely alkali metal (Li, Na, or K) and alkaline earth metal (Mg or Ca) doping, transition metal (Zn, Ni, Mn, Ti, or Co) or their oxides doping, non-metal (C or N) doping, as well as non-metal-/metal-doped composites. Metal doping molybdenum oxides are attractive as hosts for ions, which can form multiple crystal structures or phases. The combination of dissimilar metal with molybdenum oxides is able to produce materials with new architectural and chemical characteristics; thus, a variety of systems could be explored [6]. In addition, some metal-doped molybdenum oxides have a pseudocapacitive property according to the literature [16,17]. Non-metal doping is a common way of material modification, while the frame structure composed of carbon or nitrogen can greatly increase the specific surface area of the materials and enhance conductivity. Because molybdenum has different oxidation states in the compounds, molybdenum oxides doped with different elements have a variety of chemical compositions and crystal phases, and there are bound to be many synthetic methods to obtain new materials. In this review, we primarily highlight and summarize the variety of hetero-element-doped molybdenum oxide materials and their synthetic methods, as well as their electrochemical performance as energy storage materials. Figure 1 summarizes some typical crystal structures and nanostructures of hetero-element-doped molybdenum oxide materials, as well as the schematic diagram of their application in energy storage systems; the details will be introduced later.

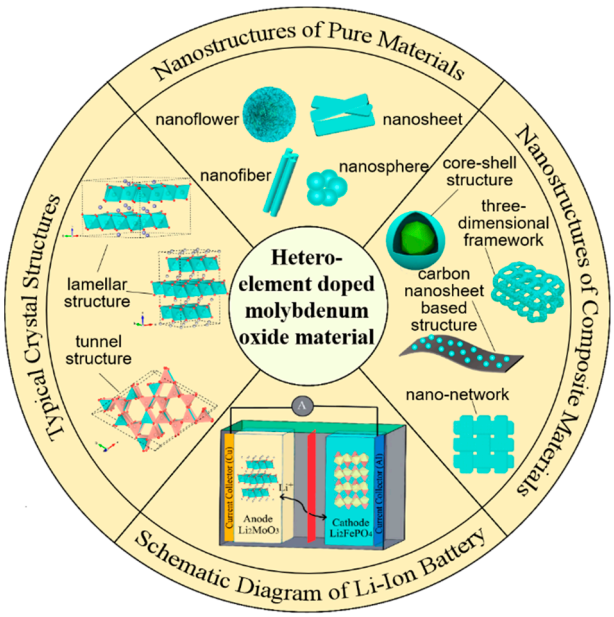

Figure 1. Summarization of some typical crystal structures and nanostructures of hetero-element-doped molybdenum oxide materials, as well as the schematic diagram of their application in energy storage systems.

2. Alkali Metal and Alkaline Earth Metal-Doped

2.1. Alkali Metal-Doped

Alkali metal-doped molybdenum oxides mainly include A_xMoO_2, A_xMoO_3, A_2MoO_4 (A = Li, Na, or K), $Li_4Mo_3O_8$, and $Li_2Mo_4O_{13}$ [18–24]. Most $LiMO_2$ (M = Co, Mn, Ni, Fe) is associated with rock-salt architectures and is an ordered or distorted form of NaCl. $AMoO_2$ (A = Li, Na or K) is isostructural to well-known $LiMO_2$ materials for LIBs, having the potential to be the lithium storage material. Per unit of MoO_2 can hold up to 0.85 Li at an average potential of 3 V [19,25]. Li_2MoO_3 has a novel, disordered α-$NaFeO_2$ structure (R-3m) with the molybdenum present as Mo_3O_{13} clusters (Figure 2b), firstly determined by James and Goodenough [26]. The Mo^{4+} in the Li_2MoO_3 compound can be oxidized to Mo^{6+} oxidation state when the Li_2MoO_3 is charged to 4.4 V (vs. Li^+/Li). Therefore, Li_2MoO_3 can carry out a two-electron electrochemical reaction per unit molecule, so it has a huge potential for energy storage (theoretical capacity is about 339 mA h g^{-1}) [27,28]. The crystal of Li_2MoO_4 (Figure 2a) shows a tunnel structure, consisting of a three-dimensional network of corner-linked, slightly distorted LiO_4 and MoO_4 tetrahedra along crystallographic c-axis [29,30]. As is well-known, materials with NASICON-type structure are also promising candidates for energy storage systems.

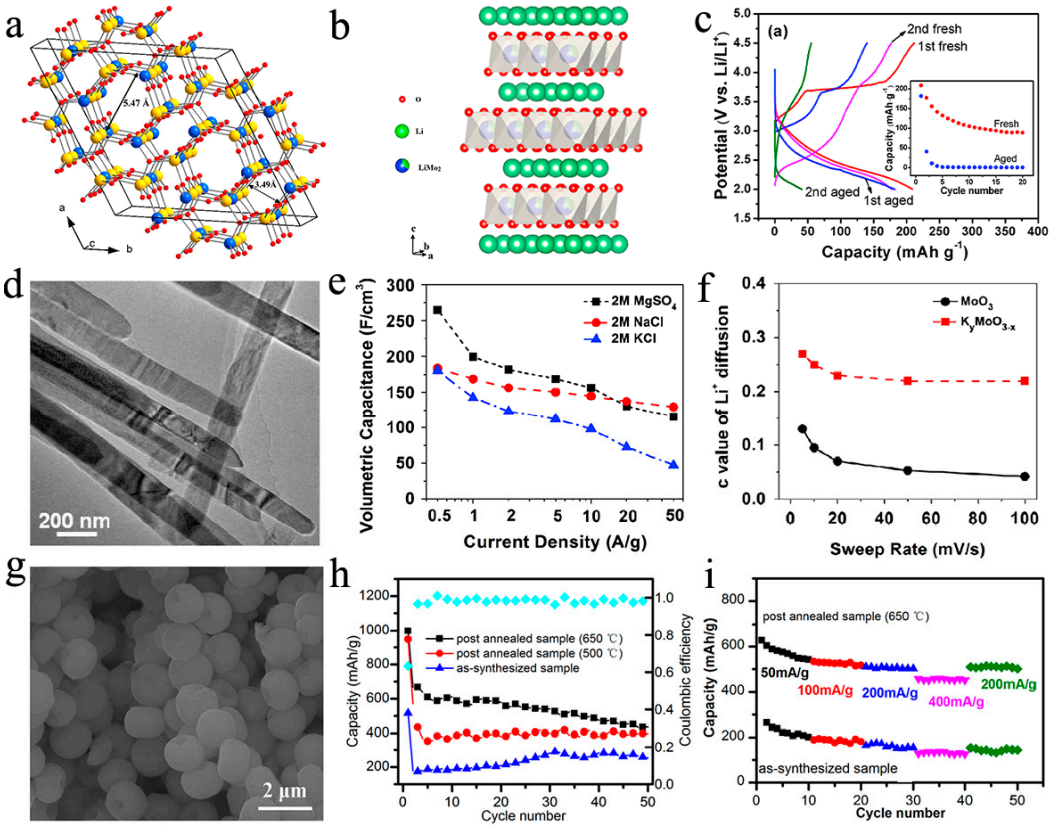

Figure 2. (**a**) Crystal structure of the rhombohedral modification of Li_2MoO_4. Blue and yellow spheres represent Mo and Li ions, respectively. Narrow and wide channels along the c-axis feature 4-member rings and 6-member rings, respectively. Reproduced with permission. [30] Copyright 2015, American Chemical Society. (**b**) Lattice structure of Li_2MoO_3. (**c**) Charge and discharge potential curves of the fresh and aged Li_2MoO_3; the inset is for their cycling performances. Reproduced with permission. [31] Copyright 2014, Elsevier B. V. (**d**) Low-resolution TEM image of K_yMoO_{3-x} nanobelts. (**e**) Volumetric capacitance and current density for K_yMoO_{3-x} in different electrolytes. (**f**) Numbers of Li^+ inserted in the tunneled MoO_3 and K_yMoO_{3-x} (c value of Li^+ diffusion). Reproduced with permission. [16] Copyright 2015, Elsevier B. V. (**g**) Morphological of as-synthesized $CaMoO_4$ microspheres by reaction time of 0.5 h. (**h**) Cycling performance of the $CaMoO_4$ microspheres before and after being heat-treated at different temperatures at current densities of 200 mA g^{-1}. (**i**) Rate performance of $CaMoO_4$ microspheres before and after calcination at 650 °C. Reproduced with permission. [32] Copyright 2018, Springer Nature.

Recently, many studies about alkali metal-doped molybdenum oxides have been reported. Ma et al. [31] investigated the structural and performance stability of Li_2MoO_3 in air. They found that Li_2MoO_3 can be oxidized/decomposed in air at room temperature. The oxidation of Mo^{4+} and the consumption of Li^+ led to the generation of Li^+ vacancies, Mo^{4+} migration, Li-Mo inversion, and the destruction of Mo_3O_{13} clusters in Li_2MoO_3. Therefore, as shown in Figure 2c, the aged material (storing the phase-pure Li_2MoO_3 in desiccators with a relative humidity of below 10% at room temperature for 120 days) delivered more attenuation of capacity after the initial cycle. Verma and coworkers [24] devised a novel procedure for the synthesis of $Li_2Mo_4O_{13}$ using a single-step conventional solid-state reaction. The rod-like (size range of 1–10 μm) material shows an initial reversible capacity of 1062 mA h g^{-1} at 0.1 C (up to theoretical capacity), and the capacity retention is 74% over 50 cycles with coulombic efficiency close to 98% during the subsequent cycles, proving that $Li_2Mo_4O_{13}$ electrodes exhibit high reversible capacity and great cycling performance. K^+ pre-intercalated hydrogenated MoO_3 (K_yMoO_{3-x}) material was reported by Xiao [16]. The MoO_3 nanobelts were synthesized using the hydrothermal method, hydrogenation was used to introduce oxygen vacancies into MoO_3 nanobelts (Figure 2d), and the resulting $MoO_{3-\delta}$ was further reacted with KBH_4. It was proved that several kinds of ions (Li^+, Na^+, K^+, and Mg^{2+}) with different ion dimensions can embed into the K_yMoO_{3-x}. In Figure 2e,f, the authors calculated volumetric capacitance at different current density for K_yMoO_{3-x} in three electrolytes, as well as the number of inserted Li^+ in K_yMoO_{3-x} and MoO_3. It is noted that Mg^{2+} has the greatest capacitance, while Na^+ has the best retaining capacitance, and, when the sweep frequency is augmented to 100 mV s^{-1}, the quantum of inserted Li^+ in K_yMoO_{3-x} remains almost invariant (from 0. 27 to 0.22), but only 0.042 Li^+ is embedded in MoO_3, demonstrating that K_yMoO_{3-x} has a wider interlayer distance and stronger conductivity compared to pure MoO_3. Zhu et al. [33] reported a novel layered sodium molybdenum oxide $Na_{0.3}MoO_2$ synthesized by solid-state reaction as an anode material for sodium-ion batteries (SIBs). The crystal and nanostructure of $Na_{0.3}MoO_2$ are both layered morphologies, and the long-term cycling performance shows an excellent capacity retention of 72.4% after 1000 cycles, and the coulombic efficiency is up to about 100%, except for the preliminary cycle.

In addition to single element doping, there are also some double elements-doped materials. In the existing research, potassium is doped in Li-rich molybdenum-based oxide or sodium molybdate. Yu et al. [34] prepared K-doped Li_2MoO_3 cathode material for the first time; the K-doped MoO_3 nanobelts were synthesized by hydrothermal method and used as templates and then annealed at high ambient temperatures. The larger K^+ could not be extracted from the interlayer during de-lithiation, staying in the Li slab to restrain the phase transformation, so the doped samples are more stable. The obtained $Li_{1.9}K_{0.1}MoO_3$ has a satisfying initial capacity (235 mA h g^{-1} at 0.05 C rate, 1C = 320 mA g^{-1}). Additionally, after a certain number of cycles, it maintains 56% of its initial capacity, which is much better than the undoped sample Li_2MoO_3 (38%). The enhanced electrochemical performance may be due to the change in the valence state of Mo^{4+} in the $Li_{1.9}K_{0.1}MoO_3$ crystal, making the sample hardly release oxygen even if it is charged to a potential of 4.4 V (vs. Li^+/Li). Serdtsev and coworkers [35] predicted the possible sodium-ion pathways and the energy barriers for sodium diffusion in the glaserite-type $A_{3-x}Na_{1+x}(MoO_4)_2$ (A = Cs, K) through the approximate bond valence sum approach. The double molybdate $K_3Na(MoO_4)_2$ has a monoclinic distorted superstructure (space group C2/c) with a quadruple unit cell, which corresponds to a much lower energy barrier for migration through the K site compared to the normal sodium site, while the ionic conductivity of sodium can be strengthened for pyrochlore doped with divalent or trivalent ions. At present, there are relatively few studies related to bimetallic elements-doped molybdenum oxide materials. However, according to the existing work, it can be seen that this strategy is expected to obtain electrode materials with a long cycle life and further improve the performance of single metal-element-doped molybdenum oxide materials.

2.2. Alkaline Earth Metal-Doped

Ca_xMoO_3, $CaMoO_4$, Mg_xMoO_3, and $MgMoO_4$ [36–39] are several common alkaline earth metal doping molybdenum oxides. $CaMoO_4$ adopts a tetragonal scheelite structure with the Mo in tetrahedral O-coordination [37]. The $CaMoO_4$ microspheres with nano-pits were synthesized through the facile hydrothermal method by You et al. [32]. The SEM of $CaMoO_4$ microspheres is shown in Figure 2g; the nano-pits distributed on the $CaMoO_4$ microspheres can alleviate the volume expansion problem and increase the specific surface area and wettability with the electrolyte, thus improving cycle stability and electrochemical performance. They discovered that the discharge capacity of $CaMoO_4$ tends to increase with increasing calcination temperature. In Figure 2h,i, for $CaMoO_4$, which is annealed at 650 °C, the leftover organic matter is fully carbonized and the best crystallinity is obtained after the high temperature treatment. When the post-annealed $CaMoO_4$ is used as anode for Li-ion battery, it has a higher reversible capacity (434 mA h g^{-1} at 200 mA g^{-1} after 50 cycles) than the theoretical capacity of graphite (372 mA h g^{-1}). The single crystals of $MgMoO_4$ displayed monoclinic symmetry and adopted the C2/m space group at normal temperature and pressure [40]. Haetge [41] reported the synthesis of templates for porous $MgMoO_4$ films with nanocrystalline walls. These materials were produced by solution phase co-assembly of chlorinated salt precursors with KLE-type poly(ethylene-co-butylene)-block-poly (ethylene oxide) di-block copolymers using the evaporation-induced self-assembly process. As the electrodes for the Li-ion battery, $MgMoO_4$ thin films deliver 162 mA h g^{-1} at C/1.5 (1C is defined as the intercalation of 1 Li^+ per formula unit in 1 h at 25 °C) after 100 cycles, and the capacity decreases only slightly between the 20th and 100th cycles. At the same time, the material employed in this work can be reversibly cycled at C/2 (175 mA h g^{-1}), 1 C (167 mA h g^{-1}), 2 C (147 mA h g^{-1}), 4 C (130 mA h g^{-1}), and 8 C (116 mA h g^{-1}) rates. It can be known that not all alkaline earth metal-doped molybdenum oxide materials can have a high capacity, although their cycling stability is relatively excellent. This may be related to the crystal structure of the material itself, which determines the material's ability to hold active ions. Of course, this is also reflected in other hetero-element-doped molybdenum oxide materials.

3. Transition Metal-Doped

Two main forms of transition metal-doped molybdenum oxides exist, namely $A_2Mo_3O_8$ and $AMoO_4$ (A = transition metal) [42–44]. $AMoO_4$ (A = transition metal), namely Mo-containing mixed oxides, are appropriate for ions to insertion, which can form multiple crystal structures or phases. The combination of dissimilar metal with molybdenum oxides is able to produce materials with new structures and chemical properties. The crystal structure of $NiMoO_4$ belongs to monoclinic crystal system (Figure 3a), and the rod-like $NiMoO_4$ produced through solution combustion synthesis was used for sodium batteries for the first time by Minakshi and coworkers [45], exhibiting a safe operation potential (~1.0 V vs. Na^+/Na). The rod crystalline phasing consists of tiny NiO grains (30 nm clusters of 10 nm grains) solidly fixed to the $NiMoO_4$ rods. The percentage of NiO rises with the quantity of oxidant, while the rods show cracks and fractures at the highest oxidant levels. These rods display a staggered morphology, allowing good surface pathways for ion exchange. Therefore, this hetero-structure material produces a high initial discharge capacity of 550 mA h g^{-1} at a current density of 0.05 A g^{-1}. In addition, it has good capacity retention of 82% after 50 cycles. Rod-shaped $MnMoO_4$ crystals with two-dimensional nanosheets have been satisfactorily produced by a new and facile wet chemical method with the help of polyvinylpyrrolidone by Liu's group [46]. Figure 3b shows the schematic diagram of the synthesis process. The rod-shaped $MnMoO_4$ is used as the work electrode for the supercapacitor and shows excellent long cycling and rate performance due to the two-dimensional nanosheets providing increased interfacial contact between the $MnMoO_4$ active material and the electrolyte, which facilitates the diffusion and charge transfer of the electrolyte. Figure 3c further illustrates the charge/discharge curves at the current density of 1 A g^{-1} for last 10 cycles (totally cycled for 1000 cycles), and

the coulombic efficiency remains nearly 100% for each cycle, with a completely reversible lithium storage process. Fei et al. [47] analyzed the electrochemical properties of α-$ZnMoO_4$ nanoparticles as anode material for Li-ion battery by a simple co-precipitation method and subsequently calcined for the first time. TEM shows the morphological property of α-$ZnMoO_4$ in Figure 3d, and the samples show a dispersed and uniform morphology with a diameter of 200–300 nm. As shown in Figure 3e, the as-prepared α-$ZnMoO_4$ exhibits excellent electrochemical performance, including a very stable capacity of 389 mA h g^{-1} at 50 mA g^{-1} with capacity loss of 0.2% per cycle for the 80th cycle. It also has excellent rate performance, and the capacity is basically restored when the current density returns to the initial value.

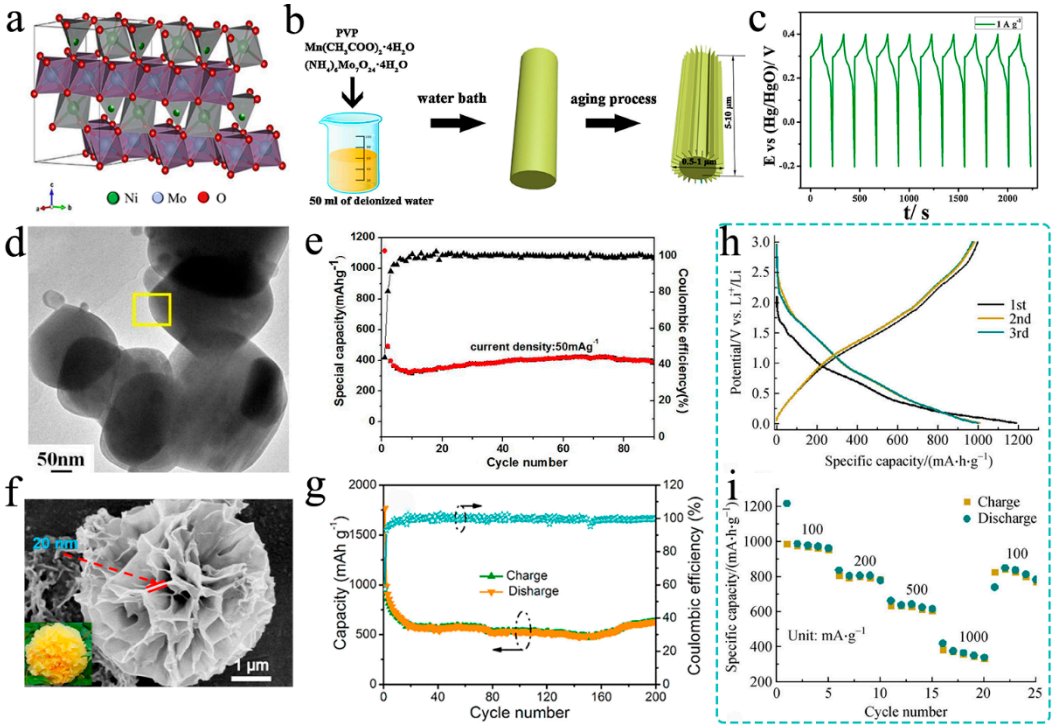

Figure 3. (**a**) Crystal structure of monoclinic $NiMoO_4$ illustrating the coordination relationship of NiO_6 and MoO_6 octahedra. Reproduced with permission. [45] Copyright 2018, Elsevier Ltd. (**b**) Schematic diagram illustrating the formation process of rod-like $MnMoO_4$ crystalline with two-dimensional nanoflakes. (**c**) GCD (galvanostatic charge–discharge) curves of the energy storage made from rod-like $MnMoO_4$ crystalline in last 10 cycles at 1A g^{-1}. Reproduced with permission. [46] Copyright 2017, Elsevier Ltd. (**d**) SEM image of α-$ZnMoO_4$. (**e**) Cycling performance of α-$ZnMoO_4$. Reproduced with permission. [47] Copyright 2017, Elsevier B. V. (**f**) SEM image of $Cu_3Mo_2O_9$. (**g**) Cycling performance and coulombic efficiency of $Cu_3Mo_2O_9$ at 0.1 A g^{-1}. Reproduced with permission. [48] Copyright 2017, Elsevier B. V. (**h**,**i**) Discharge–charge voltage profiles and rate performance of $Fe_2Mo_3O_8$ hollow spheres. Reproduced with permission. [49] Copyright 2020, Higher Education Press.

$LiHoMo_3O_8$ was prepared successfully through carbothermal reaction at 750 °C by Das et al. [50]. The Li-storage and recyclability have been examined, which delivered a high level of capacity (~470 mA h g^{-1} at 30 mA g^{-1} in rate performance) under ambient temperature. This work lays the foundation for the study and understanding of the lithium cycling mechanism of molybdenum cluster oxides and their potential applications in lithium storage devices. In the meantime, there have been many studies of isostructural Mo-cluster mixtures in which Ho is substituted by Y and possibly other heavy rare earth ions, or those in which the Li and Ho ions are substituted by two divalent metal ions, such as transition metals [42,51]. Thus, more research on the use of $A_2Mo_3O_8$ (A = transition metal) for energy storage has been reported [42,49,52,53]. Chowdari's group [42] reported the electrochemical performance and the Li-cycling mechanism of $Mn_2Mo_3O_8$ early. The

synthesized $Mn_2Mo_3O_8$ belongs to the P63mc space group and the Rietveld refined lattice parameters are: a = 5.795(2) Å and c = 10.254(2) Å. The first discharge capacity of $Mn_2Mo_3O_8$ is about 710 mA h g^{-1}, while it shows bad cycling performance. Recently, Zhang and coworkers [49] constructed novel self-assembled iron (II) molybdenum (IV) oxide hollow globules with a wall of 100 nm by a bubble-template-assisted hydrophile method of synthesis combined with simple calcination. The tight integration of miniature nanoparticles on the surface of the hollow globules not only offers more active sites for $Fe_2Mo_3O_8$ but also contributes to the stability of the hollow structure, thus enhancing the lithium storage performance. The discharge–charge voltage profiles and rate performance of $Fe_2Mo_3O_8$ hollow spheres are shown in Figure 3h,i; $Fe_2Mo_3O_8$ hollow spheres deliver the initial discharge and charge capacities of 1189 and 997 mA h g^{-1} at 100 mA g^{-1}, respectively, which are higher than the theoretical capacity of 813 mA h g^{-1} based on lithium storage mechanism of redox conversion. Additionally, in the rete performance, when the current rate decreases to 0.1 A g^{-1}, a high discharge capacity of 812 mA h g^{-1} can still be regained, suggesting the desirable tolerance of the $Fe_2Mo_3O_8$ electrode. Therefore, it is very important to improve the cycling stability and rate performance of the electrode materials by seeking suitable synthesis methods and modification methods.

In addition to these two types of transition metal-doped molybdenum oxides, $A_2Mo_3O_8$ and $AMoO_4$ (A = transition metal), $Cu_3Mo_2O_9$ used as anode for Li-ion battery was reported by Guo's group [48]. They developed a facile strategy to fabricate the 3D hierarchical $Cu_3Mo_2O_9$ flowers via simply calcining the $Cu_3(OH)_2(MoO_4)_2$ nano-cuboids, which can be accomplished easily by one-pot hydrothermal method. The final hierarchical flower-like $Cu_3Mo_2O_9$ was transferred from self-assembled rectangular parallelepiped single nanocrystal via calcination in air (SEM is shown in Figure 3f). They investigated the influence of temperature during the calcination, finding that the 3D hierarchical morphology of the $Cu_3Mo_2O_9$ annealed at 600 °C is different either from the one that is composited of irregular nanoparticles at 400 °C or from the one that is excessively aggregated at 700 °C, which is the best in these three materials. As shown in Figure 3g, after 200 cycles, the $Cu_3Mo_2O_9$ electrode was still capable of delivering a specific capacity of 632 mA h g^{-1} at 0.1 A g^{-1} with a large coulombic efficiency (~99%), demonstrating its remarkable cycling stability and reversibility. When designing experiments, we often need to set concentration gradients, temperature gradients, etc., to find the best reaction conditions. In fact, this is a very basic understanding for the synthesis of nanomaterials.

4. Non-Metal-Doped

Doping with non-metallic elements, such as carbon and nitrogen, is a typical method of electrode material modification. Carbon and nitrogen doping modification generally does not affect the crystal structure of molybdenum-based materials, but different synthesis methods, such as co-precipitation, hydrothermal technology, etc., can be used to obtain composite materials with different nanostructures. Although some molybdenum oxides possess metallic conductivity, it is necessary to improve on their electrical conductivity for better electrochemical performances. In addition, substantial volume expansion during repetitive cycling remains the key to limiting its practical deployment in lithium-ion batteries [54]. Crossbreeding with carbonaceous substrates, such as graphene, carbon nanotubes and meso/microporous carbon, carbon black, and carbon dots [55–61], is an efficient tactic to address these issues. The nanostructure of the composite material can increase the specific surface area of the material to a certain extent so that the material and the electrolyte can be more fully contacted. For doping methods, in situ synthesis, hydrothermal, calcination, etc., have been proven to be the simple and scalable approach [56,61,62]. Lu's group [60] investigated the carbon vacancy defects using density functional theory (DFT); C vacancy formation in a perfect graphene matrix was taken as a reference. When one C atom is replaced by N, the relative C vacancy formation energy becomes more negative, indicating that C atoms are gradually easier to detach, especially when replaced by bonding to N (−2.99 eV), and N doping can effectively induce C defect formation. This kind of

ability could improve the electron conductivity of electrodes and increase the active sites for ions storage. Therefore, besides doping carbon, additionally doping with nitrogen is also an effective strategy to modify materials.

In specific studies, Cao's group [63] presented a two-step hydrothermal-calcination method to produce MoO_2/N-doped graphene (MoO_2/N-GNS) hybrids, in which MoO_2 nanoparticles were homogeneously distributed on N-GNS sheets through Mo-N chemical bonds formed between MoO_2 and N-GNS (Figure 4a). Benefiting from the substrate of graphene and N-doping, the mixture has a large specific surface area (Figure 4b). As Figure 4c indicates, this material was used as an anode for Li-ion battery, delivering a high initial discharge capacity of 1517 mA h g^{-1}, and the MoO_2/N-GNS still offered a reversible capacity of up to 1139 mA h g^{-1} at 100 mA g^{-1} after 60 cycles. Three molybdenum oxide-carbon nanotube hybrid materials were investigated as the negative electrodes in an Li-ion capacitor (LICs) by Fleischmann and coworkers [64] for the first time. They compared the properties of materials with different crystal structures and morphologies obtained by annealing after deposition. The SEM of MoO_2-CNT (the best performance) is shown in Figure 4d, and flake crystals were observed in CNT networks with transverse dimensions up to 150 nm and thicknesses up to about 50 nm. Based on its excellent morphological characteristics, MoO_2-CNT negative electrodes exhibit a superior rate handling, delivering a higher maximum capacity of around 150 mA h g^{-1} compared with MoO_x-CNT and MoO_3-CNT when the current density decreased to 0.05 A g^{-1} (Figure 4e). Additionally, the calculated high power density refers to 70 Wh kg^{-1} at 83 W kg^{-1}. In fact, in molybdenum oxides, molybdenum dioxide itself has a pseudocapacitive property, so it is a matter of course that MoO_2-CNT has the best performance as the electrode for Li-ion capacitor in these three materials. This also lets us know that, sometimes, we can make assumptions about the test results based on whether the matrix material has certain properties.

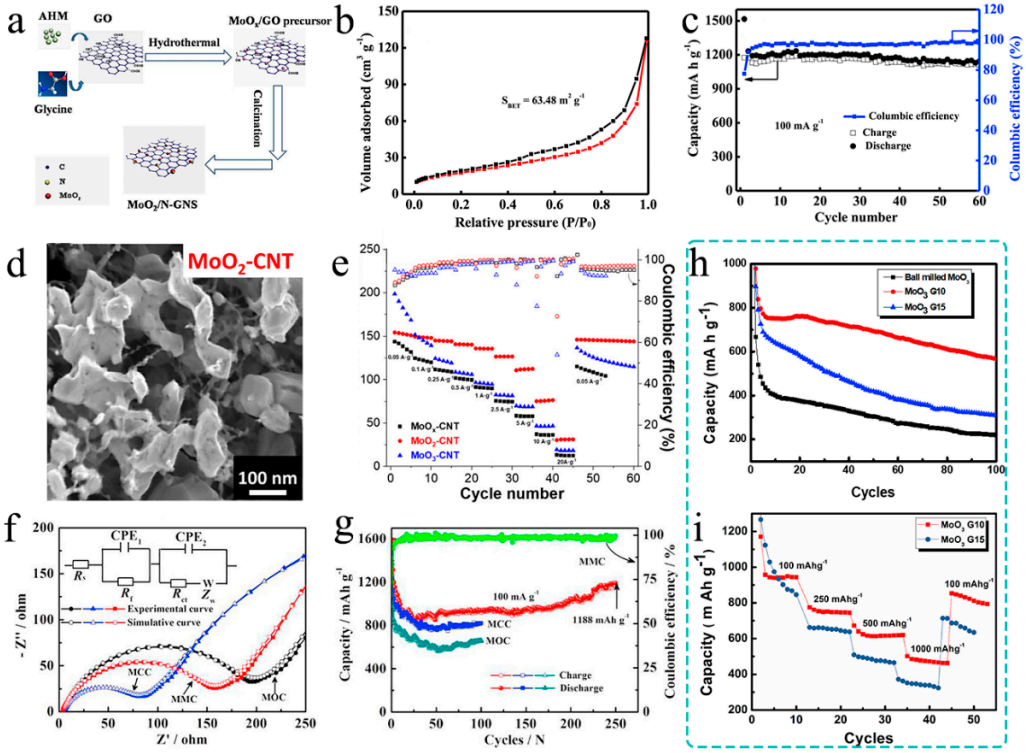

Figure 4. (**a**) Schematic illustration of the synthesis procedure of MoO_2/N-GNS hybrid. (**b**) N_2 adsorption–desorption isotherm. (**c**) Capacity vs. cycle number and the corresponding coulombic efficiency of MoO_2/N-GNS hybrid electrode. Reproduced with permission. [63] Copyright 2014, Elsevier B. V. (**d**) SEM of MoO_2-CNT after annealing at 500 °C in an argon atmosphere. (**e**) Specificde-lithiation capacity and coulombic efficiency derived from galvanostatic cycling at specific

currents between 0.05 and 20 A·g^{-1}. Reproduced with permission. [64] Copyright 2018, American Chemical Society. (**f**) The pore size distributions of MOC, MMC, and MCC samples. (**g**) The discharge–charge of MOC, MMC, and MCC samples at the current density of 100 mA g^{-1}. Reproduced with permission. [65] Copyright 2017, Elsevier B. V. (**h**) Galvanostatic tests of ball-milled MoO_3, MoO_3-10 wt % rGO, and MoO_3-15 wt % rGO. (**i**) Rate performance of MoO_3-10 wt % rGO and MoO_3-15 wt % rGO. Reproduced with permission. [66] Copyright 2019, Elsevier B.V.

For an in situ synthesis method, Chai's group [65] reported MoO_2-Mo_2C-C microspheres (MMC) synthesized via in situ carbonization as anode materials for lithium-ion batteries. Figure 4f shows the electrochemical impedance spectroscopy (EIS) of the materials. Obviously, carbon doping could reduce the charge transfer resistance, leading to a better electron conductivity, and ultimately enhance the diffusion of lithium ions to the MMC samples. Owing to the combination of the higher conductivity of Mo_2C, C and the appropriate content of Mo_2C, the MMC microspheres exhibit excellent cyclability and good stability. As shown in Figure 4g, for the MMC electrode, the initial discharge/charge specific capacities are nearly 1594/1171 mA h g^{-1} at 100 mA g^{-1}, respectively, with a relatively low coulombic efficiency of 73.5%. The loss capacity was accorded with the irreversible procedure, including the insertion of Li^+ into the MoO_2 lattice and the formation of solid electrolyte interface (SEI) film. However, this material visibly delivers an excellent discharge capacity of 1188 mA h g^{-1} after 250 cycles. Recently, Li et al. [67] produced extremely small and widely dispersed MoO_x nanoparticles anchored on N-doped three-dimensional delaminated porous carbon (3D-MoO_x@CN) based on an efficient in situ chelation and hard induction strategy. The MoO_x nanoparticles anchor on the surface of the 3D N-doped carbon with sizes between 1.5 and 3.5 nm. Therefore, the volume change during charge and discharge can be effectively mitigated, while the three-dimensional carbon skeleton can provide a conductive network, thus improving the lithium storage performance (delivering specific capacities of 742 mA h g^{-1} at current density of 100 mA g^{-1} and 431 mA h g^{-1} at 1000 mA g^{-1} after 1000 cycles, respectively).

Satyanarayana's group [66] used a facile high-energy ball-milling process followed by ultrasonication method to prepare MoO_3/rGO composites. Same as above, the composites exhibit better electrochemical performance than just nanostructured due to the increase in surface area and conductivity

Although the specific capacities of three samples drop gradually in the first five cycles, the MoO_3-10 wt % rGO sample still shows higher reversible capacity (568 mA h g^{-1} at a high current density of 500 mA g^{-1} even after 100 cycles) than commercially available graphite (Figure 4h) and good rate performance with specific capacity 502 mA h g^{-1} even at a higher current density of 1000 mA g^{-1}, and it retained the specific capacity of 853 mA h g^{-1} as the current density switched from 1000 mA g^{-1} to 100 mA g^{-1} (Figure 4i). It is conceivable that, in addition to the theoretical capacity of the material itself, enhancing the conductivity of the materials and constructing hetero-structure composite materials is very effective at improving the actual capacities and cycling stability of the electrode materials.

5. Metal and Non-Metal-Doped Composite

As previously mentioned, metal doping molybdenum oxide can change the crystal structures and phases of molybdenum oxides. If the formed metal doping molybdenum oxides have a layered crystal structure, the interlamellar spacing will increase to a certain extent. On the other hand, the crystal structure of some metal doping molybdenum oxides, such as Li_2MoO_4, is NASICON-type, which can also provide an ion storage property. Meanwhile, carbon or nitrogen doping plays a typical role in modifying materials by enhancing the electron conductivity and introducing some active sites to improve the electrochemical performance of electrode materials for ion batteries or supercapacitors. Therefore, combining the metal doping and non-metal doping has been an attractive method recently. Hu and coworkers [68] designed a carbon-coated and K-doped MoO_3 composite prepared by hydrothermal treatment followed by a high-temperature annealing to solve the problems

of low conductivity and irreversible structure change impediment. The pre-insertion of a layer of K^+ as a backbone not only provides stability to the lamellar structure but also prevents Li^+ from inserting the intralayer sites of the MoO_3 crystals [69,70]. Therefore, the reduced resistance of the modified material facilitates a performance improvement. The as-prepared $K_{0.046}MoO_3$@C composites can deliver the specific capacities of 258 and 118 mA h g^{-1} at the current densities of 30 and 3000 mA g^{-1} over the potential range of 1.5–4.0 V (vs. Li^+/Li), respectively, displaying an outstanding rate capability. When cycled at 1500 mA g^{-1}, it can retain 83.9% of the initial capacity after 500 cycles. Meanwhile, the calculated value of Li-diffusion coefficient for KMC-3 is 2.06 × 10^{-12} cm^2 s^{-1}, showing a good Li^+ diffusion efficiency.

Earlier, yolk–shell-structured microspheres composed of N-doped-carbon-coated $NiMoO_4$ hollow nanospheres (Y-$NiMoO_4$-H@C) synthesized via a spray pyrolysis process as anode for Li-ion battery was reported by Kang's group [71]. The TEM is shown in Figure 5a, and it is clear that there is the cavity in a single nanosphere. They compared the properties of hollow and dance structure of nanospheres and the samples whether in coated carbon or not. The Y-$NiMoO_4$-H@C microspheres have the largest BET surface area (55.7 m^2 g^{-1}) and show the lowest Rct value owing to the highly conductive N-doped carbon layers (Figure 5b). Obviously, yolk–shell-structured microspheres deliver great coulombic efficiency, cycling performance, and rate performance. The specific data of rate performance can be depicted in Figure 5c (final discharge capacities of 1267, 1221, 1120, 991, 907, 839, and 757 mA h g^{-1} at current densities of 0.5, 1, 2, 4, 6, 8, and 10 A g^{-1}, respectively), indicating that Y-$NiMoO_4$-H@C have fast charging and discharging processes at high current densities. Compared with the phase-pure β-$NiMoO_4$ yolk–shell sphere (719 mA h g^{-1} at 4 A g^{-1} in rate performance) [72], N-doping and carbon coating have greatly improved the capacity of $NiMoO_4$ by increasing the specific surface area and enhancing the electroconductivity.

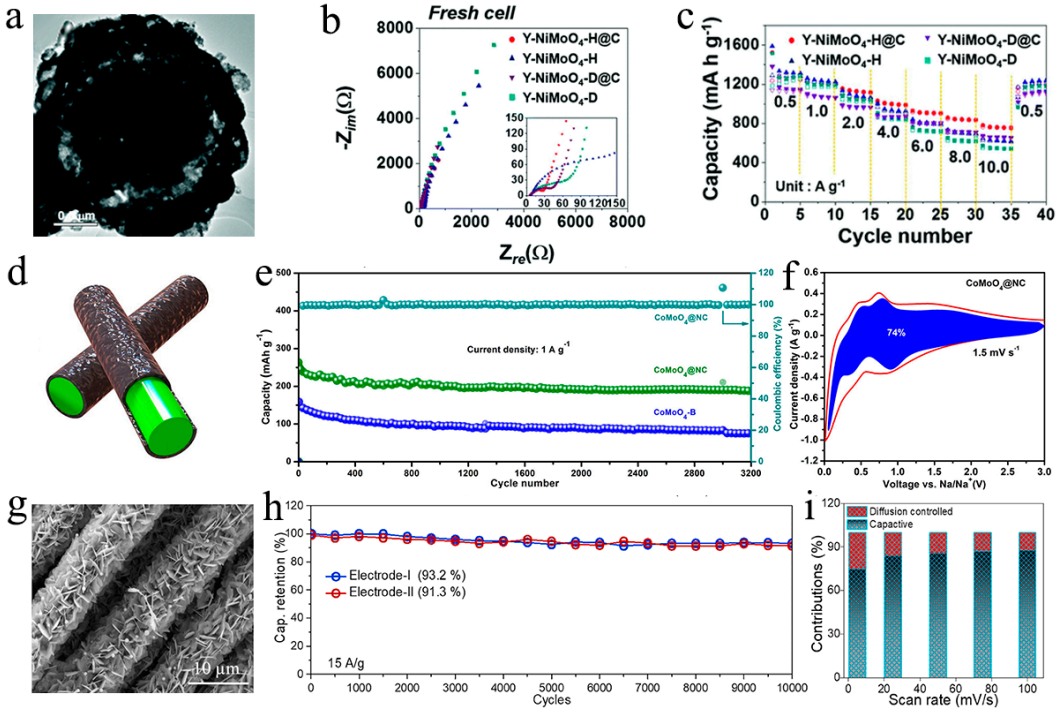

Figure 5. (**a**) TEM image of N-doped carbon coated hollow $NiMoO_4$ nanospheres. (**b**) Nyquist plots of Y-$NiMoO_4$-H@C, Y-$NiMoO_4$-H, Y-$NiMoO_4$-D, and Y-$NiMoO_4$-D@C of fresh cells. (**c**) Rate performances of Y-$NiMoO_4$-H@C. Reproduced with permission. [71] Copyright 2019, The Royal Society of Chemistry. (**d**) Schematic illustration of $CoMoO_4$@NC nanorods; the green part is rod-like $CoMoO_4$, and the coated part is N-doped carbon coatings. (**e**) Long-term cyclic performance at of

1 A g^{-1} $CoMoO_4$@NC and $CoMoO_4$-B. (**f**) The separation of the capacitive and diffusion currents of $CoMoO_4$@NC at a scan rate of 1.5 mV s^{-1}; the capacitive contribution to the total current is presented by the shaded region. Reproduced with permission. [73] Copyright 2020, Elsevier Inc. (**g**) SEM of $CoMoO_4$@CFC (hexagonal nanosheets $CoMoO_4$ are grown on the Carbon Fabric Cloth). (**h**) Cycling performance up to 10,000 cycles at current density of 15 A g^{-1} for two separate electrodes. (**i**) Capacitive and diffusive contribution at different scan rates. Reproduced with permission. [74] Copyright 2020, Elsevier Ltd. and Techna Group S.r.l.

Recently, Zhu's group [73] designed N-doped carbon-encapsulated $CoMoO_4$ ($CoMoO_4$ @NC) nanorods by a facile co-precipitation method to obtain a long-cycle-life anode material for sodium-ion battery. As shown in Figure 5d, the N-doped carbon shell acts as a cushion to adapt to gross volume changes during Na^+ insertion/extraction while enhancing the electronic conductivity and activating the surface sites of $CoMoO_4$. In fact, it shows a prolonged cycle life, especially at a high current density of 1 A g^{-1} (Figure 5e). Interestingly, the calculated capacitive current of $CoMoO_4$@NC shows that 74% of the total charge contributions are quantified as capacitive (Figure 5f). Analogously, Hussain and coworkers [74] reported a $CoMoO_4$/C composite by co-friendly hydrothermal method as a positive electrode for pseudocapacitors. Binder-free $CoMoO_4$ hexagonal nanosheets (SEM is shown in Figure 5g) were directly grown on the surface of conductive carbon fabric cloth ($CoMoO_4$@CFC), and the hexagonal-like 2D structure possesses mesoporous characteristics (BET = 68 m^2 g^{-1}) with abundant electroactive sites as the main body of charge storage. The electrochemical properties show that the material has excellent cycling stability as the capacitance retained up to 93.2% after up to 10,000 cycles, especially at a high current density of 15 A g^{-1} (Figure 5h). In addition, Figure 5i indicates the capacitive charge storage contributions at different scan rates and, accordingly, the $CoMoO_4$@CFC electrode was attributed to a high capacitive charge value of 75% at 2.5 mV s^{-1}. Using carbon-based materials as a coating layer or as a base frame material is an effective strategy for constructing new nanostructures of composite materials. At the same time, the materials with heterogeneous structure tend to have better cycling stability due to structural stability and almost having no volume expansion problem.

6. Summary and Outlook

In this review, we have attempted to chart the significant progress in hetero-element-doped molybdenum oxides for ion batteries and supercapacitors. The summarized series data and parameters of some hetero-element-doped molybdenum oxides are shown in Table 1. As can be seen from Table 1, the hetero-element-doped molybdenum oxide materials are mainly applied to the anode materials of lithium-ion batteries at present, and a small portion of them are used as the cathode materials in ion batteries and electrodes in supercapacitors. When they are applied to batteries, these materials generally have a voltage window of about 0~3.0 V. Among these hetero-element-doped molybdenum oxide materials, there is no way to make a specific comparison of different materials due to the inconsistency in the current densities and the number of cycles during the test, but the performances of these materials are much better than that of pure molybdenum oxide without doping. At the same time, the nanostructures of the materials also have a great influence on the performance. Therefore, in addition to the selection of doping elements, researchers also need to find a suitable synthesis method to obtain a nanostructure with a larger specific surface area and a small volume expansion effect.

Table 1. Summary of the properties and applications of some hetero-element-doped molybdenum oxide materials.

Active Component		Application Fields	Specific Capacity (mA h g^{-1})	Cycles	Current Density (mA g^{-1})	Voltage Window (V)	Refs.
Alkali metal	$Na_{1/3}MoO_2 \cdot H_2O$	Li/Na dual-ion battery (cathode)	650	500	50	0~3.0	[18]
	Li_2MoO_4@C	Li-ion battery (anode)	504	150	100	0.02~3.0	[75]
	$Li_2Mo_4O_{13}$	Li-ion battery (anode)	768	50	106	0.1~2.5	[24]
	Lithiated MoO_3 Nanobelts	Li-ion battery (cathode)	220	15	50	0.15~3.0	[76]
Non-metal	3D-MoO_x@CN-700	Li-ion battery (anode)	431	1000	1000	0.01~3.0	[66]
	MoO_3/NC	Li-ion battery (anode)	1250	60	410	0.01~3.0	[77]
	a-MM/NCc	Sodium-ion battery (anode)	1253	50	100	0.01~3.0	[78]
	MoOC/N-doped C	Li-ion battery (anode)	793	100	100	0.01~3.0	[79]
Transition metal or doped non-metal composites	$MnMoO_4$@C	Li-ion battery (anode)	1050	200	100	0~3.0	[54]
	$NiMoO_4$	Sodium-ion battery (anode)	245	100	50	0~3.0	[45]
	$Cu_3Mo_2O_9$	Li-ion battery (anode)	632	200	100	0.01~3.0	[53]
	$MnMoO_4/CoMoO_4$	Supercapacitor	187 (F g^{-1})	1000	1000	0.1~0.4	[80]
	$CoMoO_4$/AF-CNT	Sodium-ion battery (anode)	220	200	100	0.01~3.0	[81]
	$ZnMoO_4$/rGO	Li-ion battery (anode)	632	100	100	0.01~3.0	[82]

Doping with different elements can change the crystal structure of molybdenum oxides (enlarge the interlamellar spacing or completely convert them to tunnel-type), introduce more active sites to increase the diffusion rate of the ions in the solid phase, increase the conductivity of the material, as well as make the material structure not easy to collapse and expand. These developments have greatly enriched molybdenum oxide-based materials and pave the way for possible design ideas of commercial materials. In addition, the changes in the complex structure and composition evolution during the electrochemical reactions and ion storage mechanisms of some molybdenum oxide-based materials are clarified, although many details of the electrochemical mechanisms on molybdenum oxide-based materials remain controversial and unclear. Except for designing different doped compounds and microstructures of hetero-element-doped molybdenum oxides to improve the capacity and cyclability for energy storage systems, how to reduce irrepressible capacity is an issue that needs attention. In many studies, it has been found that the initial charge capacity is very high, and the subsequent capacity will have a large attenuation and then remain within a certain range, indicating that the coulombic efficiency of the first cycle is very low, especially in nanostructure materials. Doping with hetero-elements and confirming the synthetic process usually involves the design of nanostructures of electrode materials. It is worth noting that irreversible capacity loss is crucial to real full cells, compromising the energy density and even the effect of nanostructuring. Therefore, using the current advanced technology to find ways to improve the coulombic efficiency of the first cycle is worthy of attention. The development of hetero-element-doped molybdenum oxide materials still faces great challenges, but notable progress has been made in the past years. Significant progress has been made regarding the material synthesis, improving electrochemical performances, and understanding the charge transport mechanism used in the energy storage systems.

In order to obtain materials with better performance, in addition to continuing to try different synthesis methods to obtain single metal-element-doped molybdenum oxides

with different nanostructures, we could explore the synthesis of more bimetal-element-doped molybdenum oxide materials on the basis of the existing work [33,34], which will contribute to a significant expansion for molybdenum oxide-based materials. Based on the high capacity of different element-doped molybdenum oxide materials for lithium ions, most of the materials are now studied as anode materials for lithium-ion batteries. The active ions of other ion batteries, such as sodium-ion, potassium-ion, magnesium-ion, etc., have a larger radius than lithium-ion batteries. Therefore, hetero-element-doped molybdenum oxides may not meet the performance requirements as anodes for other ion batteries, but we could try to use them as cathode materials, which is a direction that has not been extensively studied. For non-metallic doping, there are a few cases that use materials that can be carbonized in nature as the substrate to obtain peculiar nanostructured composite materials. This is also a promising research idea; after all, nature is always worth learning from. There is no doubt that a basic understanding of the electrode structure, electrode/electrolyte interface, and charge storage mechanism, as well as a good study of the electron and ion transport in electrode/electrolytes through theoretical calculations, have important guiding significance for the development of molybdenum oxide-based materials.

Author Contributions: Investigation, B.H., S.J., G.Y., W.F., Y.C., J.B., Y.L., H.T.; writing—original draft preparation, B.H.; writing—review and editing, H.T.; visualization, S.J., G.Y., W.F., Y.C., J.B., Y.L., H.T.; supervision, Y.D.; funding acquisition, Y.D. All authors have read and agreed to the published version of the manuscript.

Funding: This work was supported by the National Key R&D Program of China (2017YFA0208000), the National Natural Science Foundation of China (22004112, 51902296).

Conflicts of Interest: The authors declare no conflict of interest.

References

1. Harper, G.; Sommerville, R.; Kendrick, E.; Driscoll, L.; Slater, P.; Stolkin, R.; Walton, A.; Christensen, P.; Heidrich, O.; Lambert, S.; et al. Recycling lithium-ion batteries from electric vehicles. *Nature* **2019**, *575*, 75–86. [CrossRef]
2. Nai, J.; Zhao, X.; Yuan, H.; Tao, X.; Guo, L. Amorphous carbon-based materials as platform for advanced high-performance anodes in lithium secondary batteries. *Nano Res.* **2021**, *14*, 2053–2066. [CrossRef]
3. Du, H.; Feng, S.; Luo, W.; Zhou, L.; Mai, L. Advanced Li-Se_xS_y battery system: Electrodes and electrolytes. *J. Mater. Sci. Technol.* **2020**, *55*, 1–15. [CrossRef]
4. Manthiram, A. An Outlook on Lithium Ion Battery Technology. *ACS Cent. Sci.* **2017**, *3*, 1063–1069. [CrossRef]
5. Kukushkin, V.Y. Thionyl chloride as comprehensive reagent in preparative inorganic and coordination chemistry. *Zhuarnal Neorg. Khimii* **1990**, *35*, 2236–2249.
6. Hu, X.; Zhang, W.; Liu, X.; Mei, Y.; Huang, Y. Nanostructured Mo-based electrode materials for electrochemical energy storage. *Chem. Soc. Rev.* **2015**, *44*, 2376–2404. [CrossRef]
7. Farsi, H.; Gobal, F.; Raissi, H.; Moghiminia, S. On the pseudocapacitive behavior of nanostructured molybdenum oxide. *J. Solid State Electr.* **2010**, *14*, 643–650. [CrossRef]
8. Zhu, J.; Li, P.; Chen, X.; Legut, D.; Fan, Y.; Zhang, R.; Lu, Y.; Cheng, X.; Zhang, Q. Rational design of graphitic-inorganic Bi-layer artificial SEI for stable lithium metal anode. *Energy Storage Mater.* **2019**, *16*, 426–433. [CrossRef]
9. Kim, H.; Kim, S.; Park, Y.; Gwon, H.; Seo, D.; Kim, Y.; Kang, K. SnO_2/graphene composite with high lithium storage capability for lithium rechargeable batteries. *Nano Res.* **2010**, *3*, 813–821. [CrossRef]
10. Zhou, L.; Wu, H.B.; Wang, Z.; Lou, X.W.D. Interconnected MoO_2 Nanocrystals with Carbon Nanocoating as High-Capacity Anode Materials for Lithium-ion Batteries. *ACS Appl. Mater. Inter.* **2011**, *3*, 4853–4857. [CrossRef] [PubMed]
11. Xuan, H.C.; Zhang, Y.Q.; Xu, Y.K.; Li, H.; Han, P.D.; Wang, D.H.; Du, Y.W. A facile route to large-scale synthesis MoO_2 and MoO_3 as electrode materials for high-performance supercapacitors. *Physic. Status Solidi* **2016**, *213*, 2468–2473. [CrossRef]
12. Vorobeva, N.S.; Lipatov, A.; Muratov, D.S.; Sinitskii, A. Chemical vapor deposition and characterization of two-dimensional molybdenum dioxide (MoO_2) nanoplatelets. *Nanotechnology* **2018**, *29*, 505707. [CrossRef]
13. Zhuang, R.; Yao, S.; Shen, X.; Li, T. Hydrothermal synthesis of mesoporous MoO_2 nanospheres as sulfur matrix for lithium sulfur battery. *J. Electroanal. Chem.* **2019**, *833*, 441–448. [CrossRef]
14. Mccrory, M.; Kumar, A.; Ram, M.K. Hydrothermal Synthesis of MoO_2 Nanoparticles Directly onto a Copper Substrate. *Mrs Adv.* **2016**, *1*, 1051–1054. [CrossRef]
15. Zhang, H.; Zeng, L.; Wu, X.; Lian, L.; Wei, M. Synthesis of MoO_2 nanosheets by an ionic liquid route and its electrochemical properties. *J. Alloy. Compd.* **2013**, *580*, 358–362. [CrossRef]

16. Xiao, X.; Zhang, C.J.; Lin, S.; Huang, L.; Hu, Z.; Cheng, Y.; Li, T.; Qiao, W.; Long, D.; Huang, Y.; et al. Intercalation of cations into partially reduced molybdenum oxide for high-rate pseudocapacitors. *Energy Storage Mater.* **2015**, *1*, 1–8. [CrossRef]
17. Tomar, A.K.; Marichi, R.B.; Singh, G.; Sharma, R.K. Enhanced electrochemical performance of anion-intercalated lanthanum molybdenum oxide pseudocapacitor electrode. *Electrochim. Acta* **2019**, *296*, 120–129. [CrossRef]
18. Li, X.; Wang, Z.; Duan, X.; Xu, L.; Yang, M.; Yuan, S.; Meng, C.; Wu, Q.; Wang, Q. A novel layered birnessite-type sodium molybdate as dual-ion electrodes for high capacity battery. *Electrochim. Acta* **2020**, *363*, 137229. [CrossRef]
19. Ben-Kamel, K.; Amdouni, N.; Groult, H.; Mauger, A.; Zaghib, K.; Julien, C.M. Structural and electrochemical properties of $LiMoO_2$. *J. Power Sources* **2012**, *202*, 314–321. [CrossRef]
20. Kobayashi, H.; Tabuchi, M.; Shikano, M.; Nishimura, Y.; Kageyama, H.; Ishida, T.; Nakamura, H.; Kurioka, Y.; Kanno, R. Synthesis and electrochemical properties of lithium molybdenum oxides. *J. Power Sources* **1999**, *81*, 524–529. [CrossRef]
21. Komaba, S. Molybdenum oxides synthesized by hydrothermal treatment of A_2MoO_4 (A=Li, Na, K) and electrochemical lithium intercalation into the oxides. *Solid State Ion.* **2002**, *152–153*, 319–326. [CrossRef]
22. Hibble, S.J.; Fawcett, I.D.; Hannon, A.C. The True Structure and Metal-Metal-Bonded Framework of $LiMo^{III}O_2$ Determined from Total Neutron Scattering. *Inorg. Chem.* **1997**, *36*, 1749–1753. [CrossRef]
23. Leroux, F.; Nazar, L.F. Uptake of lithium by layered molybdenum oxide and its tin exchanged derivatives: High volumetric capacity materials. *Solid State Ion.* **2000**, *133*, 37–50. [CrossRef]
24. Verma, R.; Park, C.; Kothandaraman, R.; Varadaraju, U.V. Ternary lithium molybdenum oxide, $Li_2Mo_4O_{13}$: A new potential anode material for high-performance rechargeable lithium-ion batteries. *Electrochim. Acta* **2017**, *258*, 1445–1452. [CrossRef]
25. Mikhailova, D.; Bramnik, N.N.; Bramnik, K.G.; Reichel, P.; Oswald, S.; Senyshyn, A.; Trots, D.M.; Ehrenberg, H. Layered Li_xMoO_2 Phases with Different Composition for Electrochemical Application: Structural Considerations. *Chem. Mater.* **2011**, *23*, 3429–3441. [CrossRef]
26. James, A.; Goodenough, J.B. Structure and bonding in Li_2MoO_3 and $Li_{2-X}MoO_3$ ($0 \leq x \leq 1.7$). *J. Solid State Chem.* **1988**, *76*, 87–96. [CrossRef]
27. Lee, J.; Urban, A.; Li, X.; Su, D.; Hautier, G.; Ceder, G. Unlocking the Potential of Cation-Disordered Oxides for Rechargeable Lithium Batteries. *Science* **2014**, *343*, 519–522. [CrossRef]
28. Ma, J.; Zhou, Y.; Gao, Y.; Yu, X.; Kong, Q.; Gu, L.; Wang, Z.; Yang, X.; Chen, L. Feasibility of Using Li_2MoO_3 in Constructing Li-Rich High Energy Density Cathode Materials. *Chem. Mater.* **2014**, *26*, 3256–3262. [CrossRef]
29. Liu, X.; Lyu, Y.; Zhang, Z.; Li, H.; Hu, Y.S.; Wang, Z.; Zhao, Y.; Kuang, Q.; Dong, Y.; Liang, Z.; et al. Nanotube Li_2MoO_4: A novel and high-capacity material as a lithium-ion battery anode. *Nanoscale* **2014**, *6*, 13660–13667. [CrossRef]
30. Mikhailova, D.; Voss, A.; Oswald, S.; Tsirlin, A.A.; Schmidt, M.; Senyshyn, A.; Eckert, J.; Ehrenberg, H. Lithium Insertion into Li_2MoO_4: Reversible Formation of Li_3MoO_4 with a Disordered Rock-Salt Structure. *Chem. Mater.* **2015**, *27*, 4485–4492. [CrossRef]
31. Ma, J.; Gao, Y.; Wang, Z.; Chen, L. Structural and electrochemical stability of Li-rich layer structured Li_2MoO_3 in air. *J. Power Sources* **2014**, *258*, 314–320. [CrossRef]
32. You, J.; Xin, L.; Yu, X.; Zhou, X.; Liu, Y. Synthesis of homogeneous $CaMoO_4$ microspheres with nanopits for high-capacity anode material in Li-ion battery. *Appl. Phys. A* **2018**, *124*, 1–8. [CrossRef]
33. Zhu, K.; Guo, S.; Yi, J.; Bai, S.; Wei, Y.; Chen, G.; Zhou, H. A new layered sodium molybdenum oxide anode for full intercalation-type sodium-ion batteries. *J. Mater. Chem. A* **2015**, *3*, 22012–22016. [CrossRef]
34. Yu, S.; Peng, C.; Li, Z.; Zhang, L.; Xiao, Q.; Lei, G.; Ding, Y. K-Doped Li-Rich Molybdenum-Based Oxide with Improved Electrochemical Properties for Lithium-Ion Batteries. *Arab. J. Sci. Eng.* **2017**, *42*, 4291–4298. [CrossRef]
35. Serdtsev, A.V.; Suetin, D.V.; Solodovnikov, S.F.; Gulyaeva, O.A.; Medvedeva, N.I. Electronic structure and sodium-ion diffusion in glaserite-type $A_{3-x}Na_{1+x}(MoO_4)_2$ (A = Cs, K) studied with first-principles calculations. *Solid State Ion.* **2020**, *357*, 115484. [CrossRef]
36. Arroyo-De, D.M.; Krich, C.; Nava-Avendano, J.; Palacin, M.R.; Barde, F. In quest of cathode materials for Ca ion batteries: The $CaMO_3$ perovskites (M = Mo, Cr, Mn, Fe, Co, and Ni). *Phys. Chem. Chem. Phys.* **2016**, *18*, 19966–19972. [CrossRef] [PubMed]
37. Sharma, N.; Shaju, K.M.; Subba Rao, G.V.; Chowdari, B.V.R.; Dong, Z.L.; White, T.J. Carbon-Coated Nanophase $CaMoO_4$ as Anode Material for Li Ion Batteries. *Chem. Mater.* **2004**, *16*, 504–512. [CrossRef]
38. Bullard, J. Structural evolution of the MoO_3(010) surface during lithium intercalation. *Solid State Ion.* **2003**, *160*, 335–349. [CrossRef]
39. Mikhailik, V.B.; Kraus, H.; Itoh, M.; Iri, D.; Uchida, M. Radiative decay of self-trapped excitons in $CaMoO_4$ and $MgMoO_4$ crystals. *J. Phys. Condens. Matter* **2005**, *17*, 7209–7218. [CrossRef]
40. Sleight, A.W.; Chamberland, B.L. Transition metal molybdates of the type $AMoO_4$. *Inorg. Chem.* **1968**, *7*, 1672–1675. [CrossRef]
41. Haetge, J.; Suchomski, C.; Brezesinski, T. Ordered Mesoporous β-$MgMoO_4$ Thin Films for Lithium-Ion Battery Applications. *Small* **2013**, *9*, 2541–2544. [CrossRef] [PubMed]
42. Das, B.; Reddy, M.V.; Krishnamoorthi, C.; Tripathy, S.; Mahendiran, R.; Rao, G.V.S.; Chowdari, B.V.R. Carbothermal synthesis, spectral and magnetic characterization and Li-cyclability of the Mo-cluster compounds, $LiYMo_3O_8$ and $Mn_2Mo_3O_8$. *Electrochim. Acta* **2009**, *54*, 3360–3373. [CrossRef]
43. Buhrmester, T.; Leyzerovich, N.N.; Bramnik, K.G.; Ehrenberg, H.; Fuess, H. Electrochemical intercalation of lithium in ternary metal molybdates $MMoO_4$ (M=Cu, Zn). *Mat. Res. Soc. Symp. Proc.* **2003**, *756*, 671–676. [CrossRef]

44. Kim, S.; Ogura, S.; Ikuta, H.; Uchimoto, Y.; Wakihara, M. Synthesis of $MnMoO_4$ as High Capacity Anode Material for Li Secondary Battery. *Chem. Lett.* **2001**, *30*, 760–761. [CrossRef]
45. Minakshi, M.; Barmi, M.; Mitchell, D.R.G.; Barlow, A.J.; Fichtner, M. Effect of oxidizer in the synthesis of NiO anchored nanostructure nickel molybdate for sodium-ion battery. *Mater. Today Energy* **2018**, *10*, 1–14. [CrossRef]
46. Cao, H.; Wu, N.; Liu, Y.; Wang, S.; Du, W.; Liu, J. Facile synthesis of rod-like manganese molybdate crystallines with two-dimentional nanoflakes for supercapacitor application. *Electrochim. Acta* **2017**, *225*, 605–613. [CrossRef]
47. Fei, J.; Sun, Q.; Li, J.; Cui, Y.; Huang, J.; Hui, W.; Hu, H. Synthesis and electrochemical performance of α-$ZnMoO_4$ nanoparticles as anode material for lithium ion batteries. *Mater. Lett.* **2017**, *198*, 4–7. [CrossRef]
48. Zhang, L.; He, W.; Liu, Y.; Ling, M.; Zheng, P.; Guo, S. 3D hierarchical flower of copper molybdate $Cu_3Mo_2O_9$: Synthesis, nanostructure and lithium storage properties. *J. Alloy. Compd.* **2017**, *723*, 512–519. [CrossRef]
49. Zhang, L.; Song, Y.; Wu, W.; Bradley, R.; Hu, Y.; Liu, Y.; Guo, S. $Fe_2Mo_3O_8$ nanoparticles self-assembling 3D mesoporous hollow spheres toward superior lithium storage properties. *Front. Chem. Sci. Eng.* **2021**, *15*, 156–163. [CrossRef]
50. Das, B.; Reddy, M.V.; Subba Rao, G.V.; Chowdari, B.V.R. Synthesis of Mo-cluster compound, $LiHoMo_3O_8$ by carbothermal reduction and its reactivity towards Li. *J. Solid State Electr.* **2008**, *12*, 953–959. [CrossRef]
51. McCarroll, W.H.; Katz, L.; Ward, R. Some Ternary Oxides of Tetravalent Molybdenum. *J. Am. Chem. Soc* **1957**, 5410. [CrossRef]
52. Sun, Y.; Hu, X.; Luo, W.; Huang, Y. Hierarchical self-assembly of $Mn_2Mo_3O_8$-graphene nanostructures and their enhanced lithium-storage properties. *J. Mater. Chem.* **2011**, *21*, 17229. [CrossRef]
53. Chu, Y.; Shi, X.; Wang, Y.; Fang, Z.; Deng, Y.; Liu, Z.; Dong, Q.; Hao, Z. High temperature solid-state synthesis of dopant-free $Fe_2Mo_3O_8$ for lithium-ion batteries. *Inorg. Chem. Commun.* **2019**, *107*, 107477. [CrossRef]
54. Guan, B.; Sun, W.; Wang, Y. Carbon-Coated $MnMoO_4$ Nanorod for High-Performance Lithium-Ion Batteries. *Electrochim. Acta* **2016**, *190*, 354–359. [CrossRef]
55. Raccichini, R.; Varzi, A.; Passerini, S.; Scrosati, B. The role of graphene for electrochemical energy storage. *Nat. Mater.* **2015**, *14*, 271–279. [CrossRef]
56. Wang, B.; Xin, H.; Li, X.; Cheng, J.; Yang, G.; Nie, F. Mesoporous CNT@TiO_2-C Nanocable with Extremely Durable High Rate Capability for Lithium-Ion Battery Anodes. *Sci. Rep.* **2015**, *4*, 3729. [CrossRef]
57. Lee, S.W.; Yabuuchi, N.; Gallant, B.M.; Chen, S.; Kim, B.; Hammond, P.T.; Shao-Horn, Y. High-power lithium batteries from functionalized carbon-nanotube electrodes. *Nat. Nanotechnol.* **2010**, *5*, 531–537. [CrossRef]
58. Fang, B.; Kim, J.H.; Kim, M.; Yu, J. Hierarchical Nanostructured Carbons with Meso–Macroporosity: Design, Characterization, and Applications. *Accounts Chem. Res.* **2013**, *46*, 1397–1406. [CrossRef]
59. Song, H.; Li, Y.; Shang, L.; Tang, Z.; Zhang, T.; Lu, S. Designed controllable nitrogen-doped carbon-dots-loaded MoP nanoparticles for boosting hydrogen evolution reaction in alkaline medium. *Nano Energy* **2020**, *72*, 104730. [CrossRef]
60. Wei, Z.; Liu, Y.; Peng, Z.; Song, H.; Liu, Z.; Liu, B.; Li, B.; Yang, B.; Lu, S. Cobalt-Ruthenium Nanoalloys Parceled in Porous Nitrogen-Doped Graphene as Highly Efficient Difunctional Catalysts for Hydrogen Evolution Reaction and Hydrolysis of Ammonia Borane. ACS Sustain. *Chem. Eng.* **2019**, *7*, 7014–7023. [CrossRef]
61. Zhang, Y.; Zhao, Z.; Chen, J.; Cheng, L.; Chang, J.; Sheng, W.; Hu, C.; Cao, S. C-doped hollow TiO_2 spheres: In situ synthesis, controlled shell thickness, and superior visible-light photocatalytic activity. *Appl. Catal. B Environ.* **2015**, *165*, 715–722. [CrossRef]
62. Pan, L.; Muhammad, T.; Ma, L.; Huang, Z.; Wang, S.; Wang, L.; Zou, J.; Zhang, X. MOF-derived C-doped ZnO prepared via a two-step calcination for efficient photocatalysis. *Appl. Catal. B Environ.* **2016**, *189*, 181–191. [CrossRef]
63. Wang, X.; Xiao, Y.; Wang, J.; Sun, L.; Cao, M. Facile fabrication of molybdenum dioxide/nitrogen-doped graphene hybrid as high performance anode material for lithium ion batteries. *J. Power Sources* **2015**, *274*, 142–148. [CrossRef]
64. Fleischmann, S.; Zeiger, M.; Quade, A.; Kruth, A.; Presser, V. Atomic Layer-Deposited Molybdenum Oxide/Carbon Nanotube Hybrid Electrodes: The Influence of Crystal Structure on Lithium-Ion Capacitor Performance. *ACS Appl. Mater. Inter.* **2018**, *10*, 18675–18684. [CrossRef]
65. Yang, X.; Li, Q.; Wang, H.; Feng, J.; Zhang, M.; Yuan, R.; Chai, Y. In-situ carbonization for template-free synthesis of MoO_2-Mo_2C-C microspheres as high-performance lithium battery anode. *Chem. Eng. J.* **2018**, *337*, 74–81. [CrossRef]
66. Naresh, N.; Jena, P.; Satyanarayana, N. Facile synthesis of MoO_3/rGO nanocomposite as anode materials for high performance lithium-ion battery applications. *J. Alloy. Compd.* **2019**, *810*, 151920. [CrossRef]
67. Li, Z.; Wang, C.; Chen, X.; Wang, X.; Li, X.; Yamauchi, Y.; Xu, X.; Wang, J.; Lin, C.; Luo, D.; et al. MoOx nanoparticles anchored on N-doped porous carbon as Li-ion battery electrode. *Chem. Eng. J.* **2020**, *381*, 122588. [CrossRef]
68. Hu, Z.; Zhang, X.; Peng, C.; Lei, G.; Li, Z. Pre-intercalation of potassium to improve the electrochemical performance of carbon-coated MoO_3 cathode materials for lithium batteries. *J. Alloy. Compd.* **2020**, *826*, 154055. [CrossRef]
69. Xia, Q.; Zhao, H.; Du, Z.; Zeng, Z.; Gao, C.; Zhang, Z.; Du, X.; Kulka, A.; Świerczek, K. Facile synthesis of MoO_3/carbon nanobelts as high-performance anode material for lithium ion batteries. *Electrochim. Acta* **2015**, *180*, 947–956. [CrossRef]
70. Noerochim, L.; Wang, J.; Wexler, D.; Chao, Z.; Liu, H. Rapid synthesis of free-standing MoO_3/Graphene films by the microwave hydrothermal method as cathode for bendable lithium batteries. *J. Power Sources* **2013**, *228*, 198–205. [CrossRef]
71. Park, G.D.; Hong, J.H.; Lee, J.; Kang, Y.C. Yolk–shell-structured microspheres composed of N-doped-carbon-coated $NiMoO_4$ hollow nanospheres as superior performance anode materials for lithium-ion batteries. *Nanoscale* **2019**, *11*, 631–638. [CrossRef]
72. Ahn, J.H.; Park, G.D.; Kang, Y.C.; Lee, J. Phase-pure β-$NiMoO_4$ yolk-shell spheres for high-performance anode materials in lithium-ion batteries. *Electrochim. Acta* **2015**, *174*, 102–110. [CrossRef]

73. Huang, X.; Zhang, W.; Zhou, C.; Yang, L.; Wang, H.; Gao, Q.; Zhu, M. N-doped carbon encapsulated $CoMoO_4$ nanorods as long-cycle life anode for sodium-ion batteries. *J. Colloid Interf. Sci.* **2020**, *576*, 176–185. [CrossRef]
74. Hussain, S.; Khan, A.J.; Arshad, M.; Javed, M.S.; Ahmad, A.; Shah, S.S.A.; Khan, M.R.; Akram, S.; Zulfiqar; Ali, S.; et al. Charge storage in binder-free 2D-hexagonal $CoMoO_4$ nanosheets as a redox active material for pseudocapacitors. *Ceram. Int.* **2021**, *47*, 8659–8667. [CrossRef]
75. Zhang, J.; Li, R.; Chen, Q.; Zhao, G.; Jia, J. Porous carbon-coated Li_2MoO_4 as high-performance anode materials for lithium-ion batteries. *Mater. Lett.* **2018**, *233*, 302–305. [CrossRef]
76. Mai, L.Q.; Hu, B.; Chen, W.; Qi, Y.Y.; Lao, C.S.; Yang, R.S.; Dai, Y.; Wang, Z.L. Lithiated MoO_3 Nanobelts with Greatly Improved Performance for Lithium Batteries. *Adv. Mater.* **2007**, *19*, 3712–3716. [CrossRef]
77. Qiu, J.; Yang, Z.; Li, Y. N-doped carbon encapsulated ultrathin MoO_3 nanosheets as superior anodes with high capacity and excellent rate capability for Li-ion batteries. *J. Mater. Chem. A* **2015**, *3*, 24245–24253. [CrossRef]
78. Zhu, K.; Wang, X.; Liu, J.; Li, S.; Wang, H.; Yang, L.; Liu, S.; Xie, T. Novel Amorphous MoS_2/MoO_3/Nitrogen-Doped Carbon Composite with Excellent Electrochemical Performance for Lithium Ion Batteries and Sodium Ion Batteries. ACS Sustain. *Chem. Eng.* **2017**, *5*, 8025–8034. [CrossRef]
79. Xiu, Z.; Kim, D.; Alfaruqi, M.H.; Song, J.; Kim, S.; Duong, P.T.; Mathew, V.; Baboo, J.P.; Kim, J. Ultrafine molybdenum oxycarbide nanoparticles embedded in N-doped carbon as a superior anode material for lithium-ion batteries. *J. Alloy. Compd.* **2017**, *696*, 143–149. [CrossRef]
80. Mai, L.Q.; Yang, F.; Zhao, Y.L.; Xu, X.; Xu, L.; Luo, Y.Z. Hierarchical $MnMoO_4$/$CoMoO_4$ heterostructured nanowires with enhanced supercapacitor performance. *Nature Commun.* **2011**, *2*, 1–5. [CrossRef]
81. Zhao, Y.; Xu, Z.; Fu, H.; Xiao, R.; Fu, M.; Yue, H.; Huang, J. Swallow-Nest Architectures with Cobalt Molybdate Particulates Fixed Constructed Carbon Nanotube Supports for Stable Sodium-Ion Battery Anode. *J. Electrochem. Soc.* **2020**, *167*, 80528. [CrossRef]
82. Xue, R.; Hong, W.; Pan, Z.; Jin, W.; Zhao, H.; Song, Y.; Zhou, J.; Liu, Y. Enhanced electrochemical performance of $ZnMoO_4$/reduced graphene oxide composites as anode materials for lithium-ion batteries. *Electrochim. Acta* **2016**, *222*, 838–844. [CrossRef]